Photoacoustics 31 (2023) 100523

Contents lists available at ScienceDirect

Photoacoustics

journal homepage: www.elsevier.com/locate/pacs

Visualizing the early-stage testicular torsion by dual-modal photoacoustic and ultrasound imaging

Mengyu Zhou [a,b,1], Luting Zhang [a,1], Jianwen Zeng [b], Yintao Lan [c], Fengbing He [a], Weijian Gao [a], Jinghang Li [a], Qian Wang [a], Weisheng Guo [a], Zhen Yuan [d,*], Jian Zhang [a,b,**]

[a] School of Biomedical Engineering, Guangzhou Medical University, Guangzhou, Guangdong, China
[b] Guangdong Engine Research Center of Urinary Continence and Reproductive Medicine, The Sixth Affiliated Hospital of Guangzhou Medical University, Qingyuan, Guangdong, China
[c] Bioland Laboratory (Guangzhou Regenerative Medicine and Health—Guangdong Laboratory), Guangzhou, Guangdong, China
[d] Faculty of Health Sciences, University of Macao, Macao, China

ARTICLE INFO

Keywords:
Testicular torsion
Photoacoustic imaging
Ultrasound imaging
Blood oxygen saturation
Torsion time

ABSTRACT

Delayed treatment of testicular torsion (TT) can lead to permanent loss of reproductive capacity. Photoacoustic imaging (PAI) and ultrasound imaging (USI) was tested for detecting TT at early stage in mice based on PAI-obtained oxygen saturation (sO_2), and USI-collected color pixel density (CPD), peak systolic velocity (PSV) and resistance index (RI). For complete TT, both CPD (9.08 % ± 3.084 to almost zero) and sO_2 data (70.09 % ± 1.656–59.84 % ± 1.427) showed an significant change 2 h post-torsion. For incomplete TT, sO_2 data exhibited a strong time relationship (Mean values: 6 h, 64.83 % ± 1.898; 12 h, 60.67 % ± 3.555; 24 h, 57.85 % ± 3.575; $P < 0.05$). However, USI-collected CPD, PSV or IR data from the same TT models showed no significant difference. This study indicated that USI and PAI could identify complete TT. Meanwhile, PAI has shown great potential in the diagnosis of incomplete TT within 24 h based on time-related sO_2 map.

1. Introduction

Testicular torsion (TT) is a typical surgical emergency that occurs in 1 in 4000 young males aged less than 25 years [1,2]. TT is caused by twisting of the testicle around the spermatic cord, resulting in decreased blood flow and oxygen supply to the testicle [3,4]. More importantly, testicular salvage rates can be up to 80–100 % or as low as 20 % when patients are surgically treated in 6 or 12 h after the injury, respectively. Therefore, development of highly sensitive methods for detection of TT, particularly in the early stages of incomplete torsion, is a key imperative. In particular, the ability to assess the duration and severity of testicular ischemia can provide distinct leverage to urologists in making the right decision about treatment. However, due to the lack of time-resolved and highly accurate imaging methods, it is very challenging to diagnose early-stage TT [5–9].

To date, the main imaging techniques used to assess TT include computed tomography (CT), magnetic resonance imaging (MRI), and ultrasound imaging (USI). However, both CT and MRI have the disadvantages of long imaging time and requiring patient cooperation; moreover, emergency access to MRI services is not always feasible [10–12]. Interestingly, color and spectral Doppler USI can effectively detect TT. However, the angle between blood flow vector and sound beam is an important factor limiting the visualization of blood flow. In addition, USI is highly operator-dependent, posing significant challenges in imaging incomplete TT [13–15]. Further, although conventional imaging modalities can roughly quantify the severity of TT, none of these can precisely capture the duration/time of torsion, particularly for early-stage TT.

By contrast, photoacoustic (PA) imaging (PAI) has exhibited advantages in visualizing both the structural and functional information of biological tissues for the detection and intervention of various diseases [16–18]. In particular, PAI as a non-invasive optical imaging technique is based on near infrared optical absorption of two major components of in vivo biological tissues, i.e., oxyhemoglobin (HbO_2) and deoxyhemoglobin (HbR), which can enable quantification of blood oxygen saturation (sO_2) in tissues [19,20]. For example, Sugiura et al.

* Corresponding author.
** Corresponding author at: School of Biomedical Engineering, Guangzhou Medical University, Guangzhou, Guangdong, China.
E-mail addresses: zhenyuan@umac.mo (Z. Yuan), jianzhang@gzhmu.edu.cn (J. Zhang).
[1] These authors contributed equally to this work.

https://doi.org/10.1016/j.pacs.2023.100523
Received 21 March 2023; Received in revised form 27 May 2023; Accepted 8 June 2023
Available online 9 June 2023

demonstrated that PAI has the capability for consecutive monitoring of oxygenation recovery after reperfusion in acute mesenteric ischemia in rats [21]. In addition, Hallasch et al. revealed that PAI was able to detect the early-stage psoriatic arthritis [22]. However, studies aimed to assess TT simultaneously using PAI and USI were rare.

The cure rate of TT is strongly related to torsion time. In this study, PAI was carried out for in vivo detection of TT based on the captured functional features of sO_2. An animal model was established and then in vivo experiments were performed to assess the time-related variation of sO_2 in twisted testicle (Fig. 1). It is expected that the present PAI study may open a new avenue for improved early-detection of TT.

2. Materials and methods

2.1. Animal models of TT

In this study, Kunming mouse (male, age 8–10 weeks, weight 35–45 g) was used to develop the animal model of TT. Surgery was conducted in mice under 1 % pentobarbital sodium anesthesia with a dose of 40 mg/kg intraperitoneally. First, vertical incision was made along the midline of scrotum under sterile conditions and then the scrotal layers were dissected till the internal spermatic fascia [23,24]. Further, the left testis and spermatic cord were exposed, followed by unilateral torsion and closure of overlaid scrotum (Supplementary material: Fig. S1A–D). The ethical clearance for this study was provided by the Institutional Animal Care and Use Committee of Guangzhou Medical University (GY2021-150).

2.2. Dual-modal photoacoustic and ultrasound imaging of TT

Dual-modal PAI and USI of TT were performed with a Vevo 3100 imaging system (Visual Sonics, Fujifilm). A broadband transducer (MX400: 18–38 MHz; center transmit: 30 MHz) was utilized for PAI with the spatial resolution up to 50 micro-meter (Fig. S2), which imaging penetration depth could be more than 10 mm (Fig. S3). In particular, dual-wavelength (750/850 nm) PAI was carried out, which was able to quantify sO_2 of biological tissues based on the distinct molar extinction coefficients of HbR and HbO_2 [25–27]. In addition, USI allowed parallel data collection of color pixel density (CPD) with color Doppler mode and concurrent peak systolic velocity (PSV) or resistance index (RI) imaging by spectral Doppler mode.

For dual modal imaging of TT, mice were anesthetized by using 1.5 % isoflurane mixed with air. Besides, mice were placed on an imaging platform and then ultrasound coupling gel was applied on testis of mice as well as the transducer cavity to ensure that no air bubble existed during imaging. Quantitative analysis of USI and PAI results was performed offline by using the Vevo Lab Software 3.2.0.

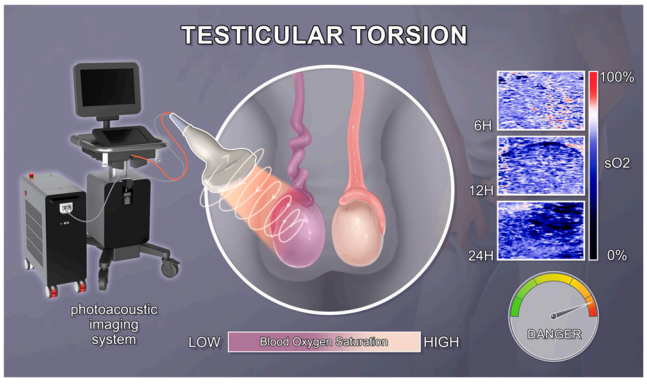

Fig. 1. Schematic illustration of the procedure for photoacoustic imaging of testicular torsion.

2.3. Experimental protocol

After torsion, 0–6 h and 0–24 h are the optimal treatment times for complete and incomplete TT, respectively [28]. Consequently, this study carried out two experimental sections, focusing on the detection of complete TT within 6 h and the evaluation of incomplete TT within 24 h with PAI and USI. In the first experimental section, the mice (n = 24) were randomly separated into four subgroups with the left testicle twisted at 0°, 90°, 180° and 360°, respectively (n = 6/group). Then, a simultaneous USI and PAI were performed before the torsion (0 h) as well as at 2 h, 4 h and 6 h after the torsion to monitor the sO_2 and CPD changes in the left testicle.

In the second experimental section, the left testicles of 18 mice were twisted between 90° and 180° with incomplete torsion and randomized to three groups (n = 6/group). Nine additional mice without surgical intervention were used as a control group. In addition, the map of sO_2 captured by PAI and PSV and RI images generated by USI were presented at 6 h, 12 h and 24 h post-torsion, respectively.

2.4. Statistical analysis

Statistical analysis of the CPD, PSV, RI and sO_2 data of normal control group and incomplete TT groups (6 h, 12 h, 24 h) in the second experimental section was respectively carried out by using SPSS software (IBM Corporation, version 21.0). CPD data obtained with USI from the left and right testes in incomplete TT groups was assessed Wilcoxon signed rank sum test. The difference in PSV, RI and sO_2 data between normal control group and the three incomplete TT groups (6 h, 12 h, and 24 h) were identified by using the Kruskal-Wallis test followed by the Kruskal-Wallis one-way analysis for multiple comparisons. Statistical significance was set at $P < 0.05$.

3. Results

3.1. Color Doppler characterizing the TT models in six hours

Torsion for six hours is the cut-off point for efficient treatment of the complete TT. In the first experimental section, a control group and three sub-groups of TT models with different torsion angle (90°, 180° and 360°) were inspected by USI at 0 h, 2 h, 4 h, and 6 h post-torsion. In particular, the quantitative blood flow within twisted testes were visualized by color Doppler USI (Fig. 2(a)). During the six-hour assessment, blood flow in the testes of control group remained steady. It was discovered that TT sub-groups at 90° and 180° exhibited blood flow in the testis, while the 360° group showed no blood flow 2 h post-torsion. To accurately quantify the changes of blood flow over time, CPD in testicular parenchyma regions was calculated and displayed in Fig. 2(b). Before TT at 0 h, CPD for the four sub-groups were 9.363 % ± 4.557, 11.04 % ± 2.213, 10.90 % ± 2.988 %, and 9.08 % ± 3.084, respectively. However, CPD for the TT three groups decreased to 5.82 % ± 2.496, 4.14 % ± 2.124 %, and 0.16 % ± 0.379, respectively, 2 h post-torsion. Further, 2–6 h post-torsion, CPD for 90° group remained at about 6.5 % and 180° group deceased to 2.75 % ± 1.598, while that of 360° group deceased to zero.

3.2. PAI mapping blood oxygen saturation of TT models in six hours

Shortly after the color Doppler USI examination, the sO_2 distribution in the testes of the control group and TT groups was collected by using PAI. As shown in Fig. 3(a), the first column was the ultrasonic image of the testes for showing the structural information. The testicular area in the sO_2 maps was marked with dashed curves. For the control group, the distribution of sO_2 in the testes remained uniform without significant hypoxia zones within six hours. By contrast, the sO_2 for the 360° group deceased more significantly 2 h post-torsion as compared to those of the 90° and 180° groups. With increased torsion time, serious hypoxia zones

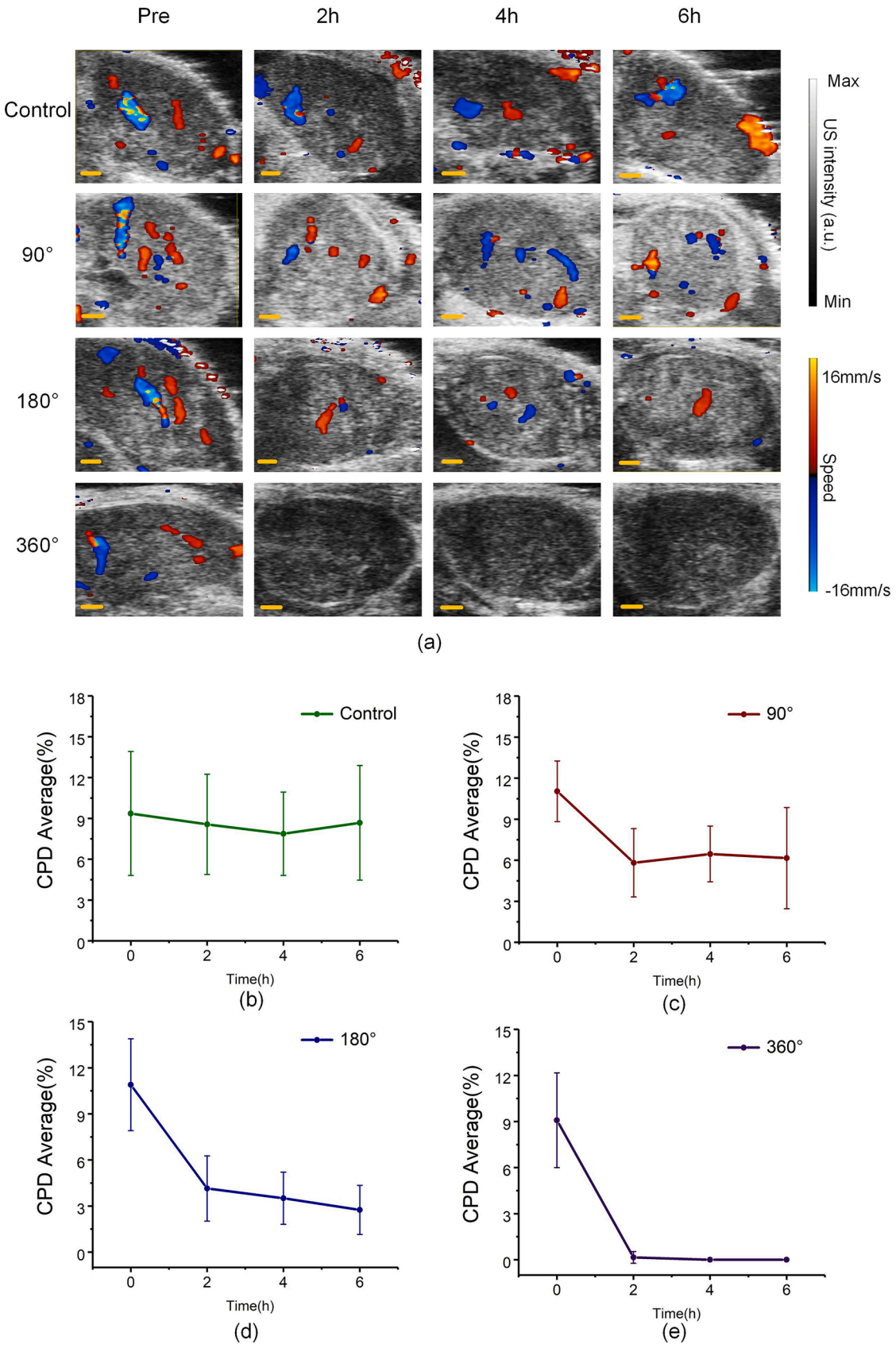

Fig. 2. USI showing blood flow of early-stage TT models. (a) Representative color Doppler images of control group and three TT groups (90°, 180°, and 360°) before and post (2 h, 4 h, 6 h) torsion. (b), (c), (d) and (e) represent the relative CPD of four groups (control, 90°, 180°, and 360°). Scale bars represent 1 mm.

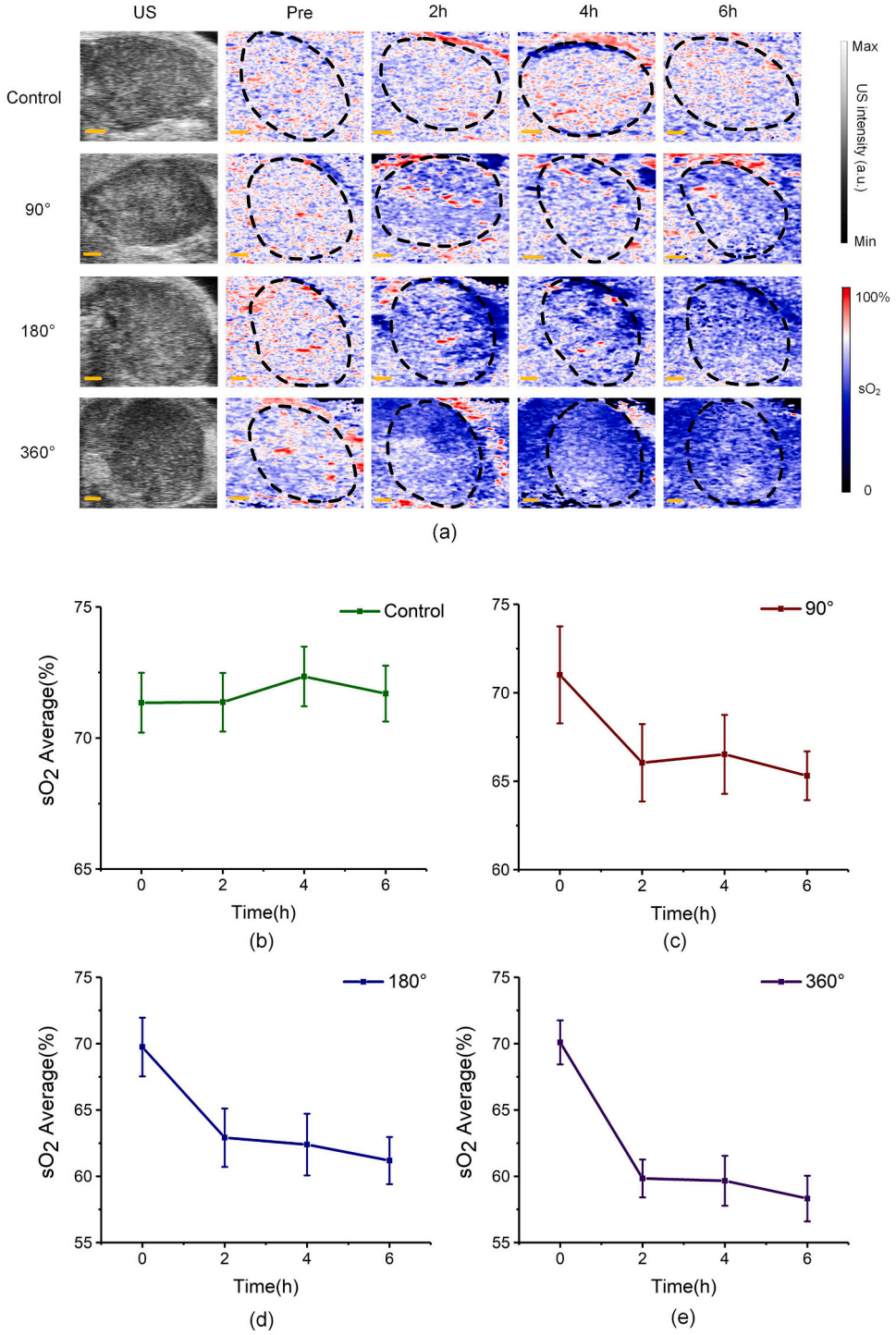

Fig. 3. PAI showing blood oxygen saturation (sO_2) of early-stage TT models. (a) Representative US and sO_2 images of control group and three groups at pre-torsion and post-torsion (2 h, 4 h, 6 h). Testicular parenchyma regions are represented by dashed line. (b), (c), (d) and (e) represent the relative sO_2 of four groups (control, 90°, 180°, and 360°) Scale bars represent 1 mm.

appeared at the edge of testis for all three TT sub-groups. Quantitative evaluation of sO_2 within the twisted testes was further performed and the analysis results were presented in Fig. 3(b). Interestingly, for the 90° group, the sO_2 decreased by 4.97 % for the first two hours after torsion and maintained around 65.5 % for the next four hours (Mean sO_2: PRE, 71.01 % ± 2.742; 2 h, 66.04 % ± 2.184; 4 h, 66.53 % ± 2.233; 6 h, 65.31 % ± 1.378). For the 180° group, the sO_2 first decreased by 6.84 % in the first two hours, and then further decreased by 1.71 % for the next four hours (Mean sO_2: PRE, 69.75 % ± 2.211; 2 h, 62.91 % ± 2.202; 4 h, 62.39 % ± 2.326; 6 h, 61.2 % ± 1.776). By contrast, for the 360° group, the sO_2 decreased by 10.26 % in the first two hours, and then further decreased by 1.52 % for the next four hours (Mean sO_2: PRE, 70.09 % ± 1.656; 2 h, 59.84 % ± 1.427; 4 h, 59.66 % ± 1.882; 6 h, 58.32 % ± 1.717). Meanwhile, the sO_2 map of the control group fluctuated around 71% within six hours (Mean sO_2: PRE, 71.35 % ± 1.141; 2 h, 71.37 % ± 1.118; 4 h, 72.35 % ± 1.138; 6 h, 71.695 % ± 1.067).

3.3. Long-term characterizing incomplete TT by color Doppler USI

The optimal surgical time for incomplete TT is longer than that of complete TT. Therefore, in the second experimental section, incomplete (90–180°) TT models were identified by twisting the left testicle. Subsequently, a long-term assessment from 6 h to 24 h after the torsion was performed. The bilateral testicular blood flow parameter for the three incomplete TT models (n = 6 per group) was captured by color Doppler USI at 6 h, 12 h, or 24 h post-torsion. As can be seen in Fig. 4(a) the blood flow in the normal (right) testis and the torsion (left) testis showed little difference. Otherwise, the blood flow differential between the three detection points is negligible. Furthermore, quantitative CPD data (Fig. 4(b)) was also calculated (Mean CPD: 6 h-left, 5.943 % ± 2.358; 6 h-right, 6.94 % ± 3.901; 12 h-left, 5.73 % ± 2.460; 12 h-right, 4.99 % ± 2.749; 24 h-left, 6.11 % ± 3.134; 24 h-right, 5.80 % ± 3.346), which showed no significance (P = 0.795).

3.4. Long-term imaging incomplete TT with spectral Doppler USI

For further evaluation, USI Doppler spectral technology was used to access the status of incomplete TT models in the second experimental section. As shown in Fig. 5(a), the spectral waveform of the artery within the incomplete twisted testicle showed low resistance and high flow compared with those of the normal testicle. Quantitative calculation was performed to generate PSV data and RI data of the normal control and TT subgroups based on the spectral Doppler ultrasonic images. As shown in Fig. 5(b), PSV data (Median value: normal group, 64.12 mm/s; group-6 h, 41.88 mm/s; group-12 h, 34.135 mm/s; group-24 h, 41.695) and the RI data (Median value: normal group, 0.36; group-6 h, 0.345; group-12 h, 0.385; group-24 h, 0.335) were further analyzed to assess the difference separately. However, the difference among the groups in the PSV (P = 0.094) and RI (P = 0.969) data was not significant (P > 0.05).

3.5. Long-term monitoring the sO_2 of incomplete TT by PAI

For patients with incomplete TT, the rule of change of sO_2 on the affected testis within 24 h is not known. It is important to monitor changes in structural and functional information over the 24 h following the TT. Therefore, quantitative PAI was performed to capture the sO_2 changes over a longer time window (24 h). As shown in Fig. 6(a), the incomplete TT group showed a significant reduction in sO_2 over time from normal controls. The results of the quantitative analysis were presented in Fig. 6(b), showing that the sO_2 decreased with increased TT time (Mean sO_2: normal group, 69.11 % ± 0.997; group-6 h, 64.83 % ± 1.898; group-12 h, 60.67 % ± 3.555; group-24 h, 57.85 % ± 3.575; P < 0.05). The statistical analysis results demonstrated a significant difference between the normal group and three incomplete TT groups (P = 0.0001). The sO_2 data at 6 h after twisting also showed a significant difference (P = 0.012) from those obtained at 12 h and 24 h. But the data of sO_2 collected from 12 h or 24 h TT show no significance (P = 0.337).

4. Discussion

TT is a urological emergency requiring immediate diagnostic evaluation. Torsion time and torsion angle are critical parameters for guiding treatment decision-making [3,9].

For patients with early onset TT who have not yet acquired language skills, It is difficult for the urologist to determine the duration of symptoms and therefore unable to assess the severity of testicular injury. USI is an efficient, practical, radiation-free and noninvasive method to diagnose TT. Despite the high diagnostic accuracy of USI for complete TT, it may lead to false-negative diagnoses in cases of incomplete TT [13,29–32]. As a novel imaging technique, PAI can exploit an sO_2 map of tissue to offer more valuable information [33]. Herein, This study performed an animal model-based study to clarify the effect of PAI in the monitoring of testicular ischemia. The data presented evidence that PAI could realize the diagnosis of TT provide a positive correlation to USI analysis and display more advantages compared with USI in cases of incomplete TT.

In the first experimental section, a control group and three TT model groups (90°, 180° and 360°) were evaluated with USI and PAI at the early stage (0 h, 2 h, 4 h and 6 h). Perhaps from a slight torsion, the quantitative data of CPD and sO_2 in the 90° incomplete TT group showed decline in the first two hours and slight fluctuations in the next four hours after torsion (Fig. 2, Fig. 3). Compared to the control group, the sO_2 images of 90° group showed the clear hypoxia zone along the edge of the testicles over time. Meanwhile, CPD results and sO_2 results from the other incomplete TT group (180°) showed a reduction in temporal correlation. In most cases, there was still the red hyperoxia zone in the sO_2 map of the testicles of the incomplete (90° and 180°) groups, which was different from the 360° group within 6 h after torsion. Incomplete testicular torsion could evolve towards complete torsion over time [34]. In this case, USI results combined with USI results and clinical symptoms

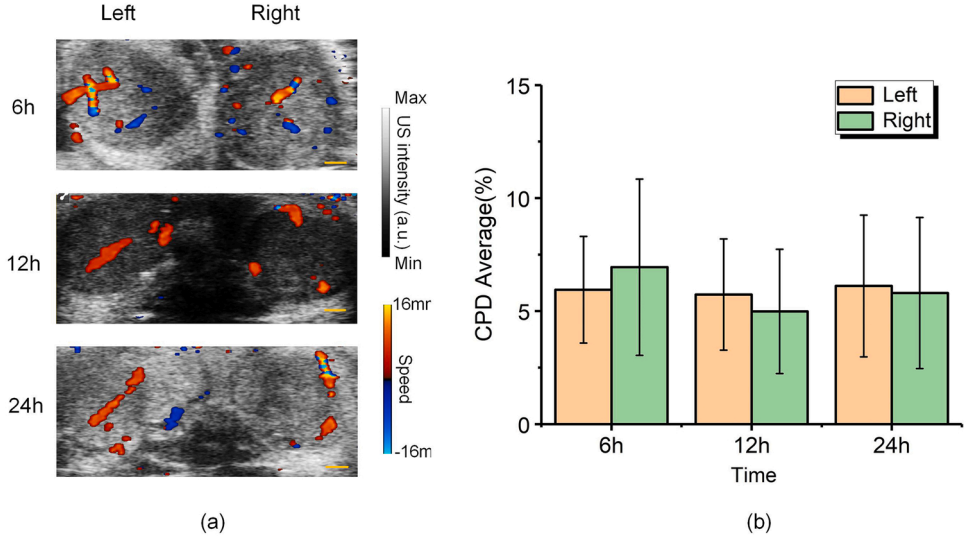

Fig. 4. Color Doppler USI evaluation of incomplete TT model for longer terms. (a) Color Doppler images of bilateral testes at 6 h, 12 h, or 24 h after surgery. Torsion of left testis, right testis not twisted. (b) Quantification of intra-testicular blood supply. Scale bars represent 1 mm.

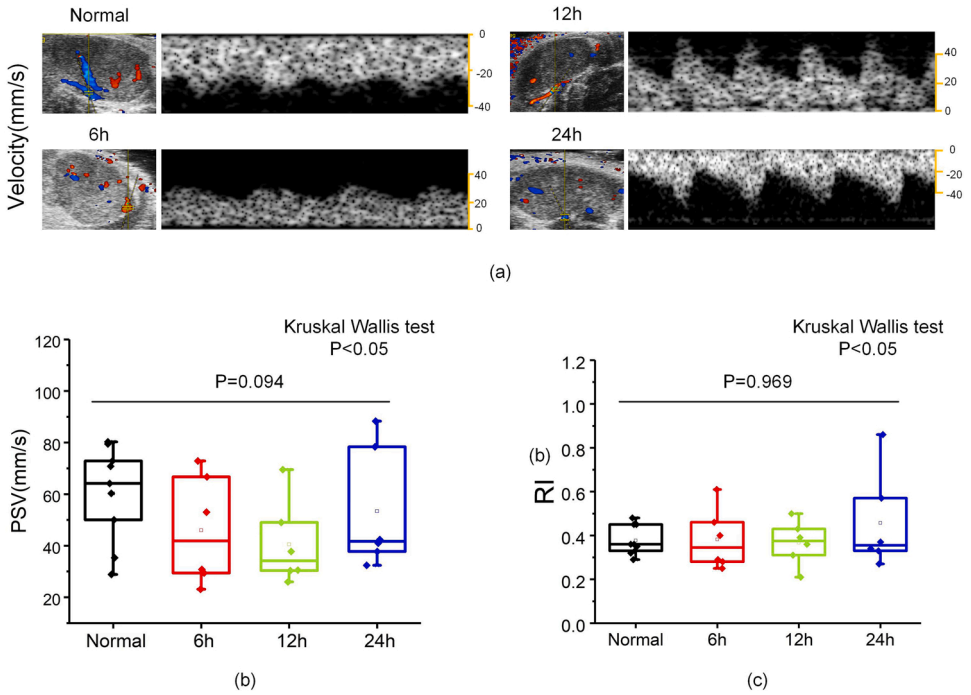

Fig. 5. Spectral Doppler USI evaluation of incomplete TT models at 6 h, 12 h, and 24 h. (a) Spectral Doppler USI images of normal testis and incomplete TT models at 6 h, 12 h, and 24 h. (b) Box diagram for peak velocity (PSV) of testicular artery. (c) Box diagram for the resistive index (RI) of testicular artery. Note: Values are expressed as box and whiskers plots; the minimum and the maximum value (whiskers), and the 25th and 75th percentile (box).

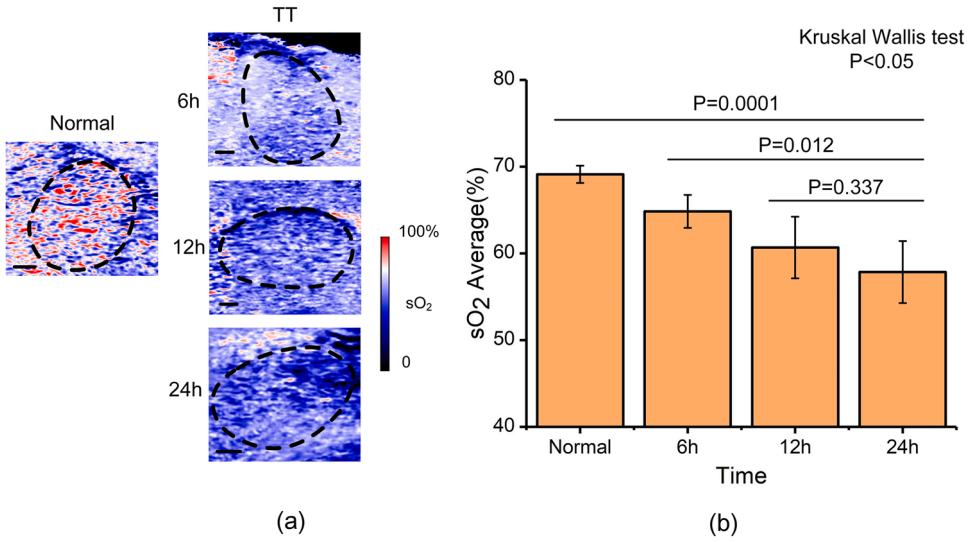

Fig. 6. Long-term PAI evaluation of the blood oxygen saturation in incomplete TT model. (a) sO_2 images of normal and incomplete TT models at 6 h, 12 h, and 24 h. Testicular parenchyma regions are represented by black dashed line. The arrows indicate the areas with low sO_2. (b) Quantitative Analysis results of sO_2 images. Scale bars represent 1 mm.

could be considered in a comprehensive manner to prevent unnecessary orchiectomy. In addition, the CPD data of complete TT (360°) group remained at zero after two hours of twisting, which failed to provide torsion time message for surgeons. However, the sO_2 results of complete torsion group showed a better time correlation than USI results. The first experimental section results confirmed that USI was an effective technology for identifying complete TT. Combination of USI results with the PAI results could provide more valuable information about torsion time of complete TT at early stage.

For incomplete TT, the affected testicle may still be salvaged within 24 h. To give a comprehensive test of PAI in the diagnosis of incomplete TT, a time-extension (6 h, 12 h and 24 h) incomplete TT model (90–180°) based the second experimental section was performed in this study. Color Doppler and spectral Doppler were first used to assess incomplete TT. Color Doppler results of bilateral testicles (Fig. 4) demonstrate a symmetric color flow. The real-time blood flow results displayed by Doppler did not change significantly ($P = 0.795$) between left and right testicle. Spectral Doppler results of twisted testes (Fig. 5) demonstrated a high flow, low resistance epididymal arterial waveform. However, there was no significant difference spectral Doppler (RI and PSV) results at 6 h, 12 h and 24 h after partial torsion of testis compared with the data from control group ($P > 0.05$). The quantitative analyzing result demonstrated that neither color Doppler data or spectral Doppler data could be used for identifying the torsion time of incomplete TT from

6 h to 24 h. Because it is difficult to detect blood flow signals of infants due to small testicular volume. Chances are that TT may be misdiagnosed as negative under this condition.

PAI results of the same incomplete TT groups showed valuable phenomenon. With the increase of torsion time (6 h, 12 h and 24 h), area of low blood oxygen could be seen in the sO_2 maps (Fig. 6). Further quantitative analysis demonstrated that the sO_2 difference was statistically significant and had perfect time correlation. These results indicated that the torsion time of incomplete TT could be identified according to the PAI results, which will be very conducive to the rescue of neonatal TT. Previous studies demonstrated that near-infrared spectroscopy could provide several valuable indexes for diagnosing TT from the perspective of sO_2. However, near-infrared spectroscopy is a directly measuring mode that only enables the evaluation of sO_2 variation, failing to offer anatomical information [35–37].

As a hybrid imaging technique, PAI/USI system integrates the advantages of optical contrast and ultrasonic resolution, allowing parallel collection of anatomical and functional information [38–40]. It can simultaneously demonstrate the spatial distribution of hypoxia area and the mean sO_2 in testes, which could help surgeons in roughly estimating the duration of testicular and deciding on an appropriate surgical treatment. In addition, the PAI is less challenging to operate, reducing the time spent in the detection process and doctor experience requirements.

While this work provides favorable evidence of PAI detecting early-stage TT, its application to clinical practice remains technically limited. Firstly, People with different skin colors may have an impact on the results of PAI. In order to eliminate skin color interference, some image processing algorithms should be considered [41,42]. Secondly, although this pilot study supports the development of PAI as a preoperative diagnostic tool for acute TT, there are still technical limitations and a lack of clinical equipment standardization. More portable and user-friendly clinical PAI systems need to be developed in the future.

5. Conclusion

This study suggests the feasibility of PAI for the diagnosis of TT at early stage, in which PAI was found to accurately represent the sO_2 map in the TT model over time.

CRediT authorship contribution statement

MZ and LZ contributed equally to this work. JZ and ZY were the supervisors of this research. All authors contributed to the study conception and design. Data collection and analysis were performed by MZ and LZ. Material preparation and Methodology were performed by J-WZ, YL, FH, WG, JL, QW and WG. The first draft of the manuscript was written by MZ and LZ, all authors commented on previous versions of the manuscript. All authors read and approved the final manuscript.

Declaration of Competing Interest

The authors declare that they have no known competing financial interests or personal relationships that could have appeared to influence the work reported in this paper.

Data Availability

Data will be made available on request.

Acknowledgments

This research was supported by the National Key R&D Program of China (2022YFC2304205).

Appendix A. Supporting information

Supplementary data associated with this article can be found in the online version at doi:10.1016/j.pacs.2023.100523.

References

[1] A. Gupta, A. Croake, D. Rubens, et al., Do not get it twisted: common and uncommon manifestations of testicular torsion, J. Ultrasound Med. 41 (2022) 271–283, https://doi.org/10.1002/jum.15723.
[2] C. Desai, K. Raghuvanshi, H. Panesar, et al., Importance of touch: managing testicular torsion in a 28-year-old with duchenne muscular dystrophy, Cureus 14 (2022), e22775, https://doi.org/10.7759/cureus.22775.
[3] L.B. Mellick, J.E. Sinex, R.W. Gibson, et al., A systematic review of testicle survival time after a torsion event, Pediatr. Emerg. Care 2019 (35) (2019) 821–825, https://doi.org/10.1097/PEC.0000000000001287.
[4] Y. Takahashi, H. Kioka, S. Saito, et al., Accurate estimation of the duration of testicular ischemia using creatine chemical exchange saturation transfer (CrCEST) imaging, J. Magn. Reson. Imaging 53 (2021) 1559–1567, https://doi.org/10.1002/jmri.27456.
[5] D.E. Sweet, M.K. Feldman, E.M. Remer, Imaging of the acute scrotum: keys to a rapid diagnosis of acute scrotal disorders, Abdom. Radiol. 45 (2020) 2063–2081, https://doi.org/10.1007/s00261-019-02333-4.
[6] J.B. Bass, K.S. Couperus, J.L. Pfaff, et al., A pair of testicular torsion medicolegal cases with caveats: the ball's in your court, Clin. Pract. Cases Emerg. Med. 2 (2018) 283–285, https://doi.org/10.5811/cpcem.2018.10.39497.
[7] S. Hirai, N. Hatayama, M. Naito, et al., Pathological effect of arterial ischaemia and venous congestion on rat testes, Sci. Rep. 7 (2017) 5422, https://doi.org/10.1038/s41598-017-05880-2.
[8] A.C. Dias Filho, R. Oliveira Rodrigues, C.L. Riccetto, et al., Improving organ salvage in testicular torsion: comparative study of patients undergoing vs not undergoing preoperative manual detorsion, J. Urol. 197 (2017) 811–817, https://doi.org/10.1016/j.juro.2016.09.087.
[9] L.B. Mellick, Torsion of the testicle: it is time to stop tossing the dice, Pediatr. Emerg. Care 28 (2012) 80–86, https://doi.org/10.1097/PEC.0b013e31823f5ed9.
[10] I. Daimiel Naranjo, A. Alcalá-Galiano Rubio, Inguinoscrotal pathology on computed tomography: an alternative perspective, Can. Assoc. Radiol. J. 67 (2016) 225–233, https://doi.org/10.1016/j.carj.2015.11.002.
[11] C. He, X. Zhou, J. Cheng, et al., Diffusion tensor imaging in evaluating testicular injury after unilateral testicular torsion and detorsion in rat model: a preliminary study, Andrologia 53 (2021), e14012, https://doi.org/10.1111/and.14012.
[12] F.H. Cassidy, K.M. Ishioka, C.J. McMahon, et al., MR imaging of scrotal tumors and pseudotumors, Radiographics 30 (2010) 665–683, https://doi.org/10.1148/rg.303095049.
[13] E.B. Cigsar Kuzu, M.O. Oztan, N. Guney, et al., Reassessment of a decade of experience on testicular torsion: are we making a mistake? Urol. Int. 106 (2022) 1100–1106, https://doi.org/10.1159/000525264.
[14] A.N. Bandarkar, A.R. Blask, Testicular torsion with preserved flow: key sonographic features and value-added approach to diagnosis, Pediatr. Radiol. 48 (2018) 735–744, https://doi.org/10.1007/s00247-018-4093-0.
[15] K. Ota, K. Fukui, K. Oba, et al., The role of ultrasound imaging in adult patients with testicular torsion: a systematic review and meta-analysis, J. Med. Ultrason. 46 (2019) 325–334, https://doi.org/10.1007/s10396-019-00937-3.
[16] Z. Wang, F. Yang, W. Zhang, et al., Quantitative and anatomical imaging of human skin by noninvasive photoacoustic dermoscopy, Bio Protoc. 12 (2022), e4372, https://doi.org/10.21769/BioProtoc.4372.
[17] J. Lv, Y. Xu, L. Xu, et al., Quantitative functional evaluation of liver fibrosis in mice with dynamic contrast-enhanced photoacoustic imaging, Radiology 300 (2021) 89–97, https://doi.org/10.1148/radiol.2021204134.
[18] J. Zhang, F. Duan, Y. Liu, et al., High-resolution photoacoustic tomography for early-stage cancer detection and its clinical translation, Radiol. Imaging Cancer 2 (2020), e190030, https://doi.org/10.1148/rycan.2020190030.
[19] R. Cao, A. Tran, J. Li, et al., Hemodynamic and oxygen-metabolic responses of the awake mouse brain to hypercapnia revealed by multi-parametric photoacoustic microscopy, J. Cereb. Blood Flow Metab. 41 (2021) 2628–2639, https://doi.org/10.1177/0271678X211010352.
[20] N. Sun, S. Zheng, D.L. Rosin, N. Poudel, et al., Development of a photoacoustic microscopy technique to assess peritubular capillary function and oxygen metabolism in the mouse kidney, Kidney Int. 100 (2021) 613–620, https://doi.org/10.1016/j.kint.2021.06.018.
[21] T. Sugiura, K. Okumura, J. Matsumoto, et al., Predicting intestinal viability by consecutive photoacoustic monitoring of oxygenation recovery after reperfusion in acute mesenteric ischemia in rats, Sci. Rep. 11 (2021) 19474, https://doi.org/10.1038/s41598-021-98904-x.
[22] S. Hallasch, N. Giese, I. Stoffels, et al., Multispectral optoacoustic tomography might be a helpful tool for noninvasive early diagnosis of psoriatic arthritis, Photoacoustics 21 (2020), 100225, https://doi.org/10.1016/j.pacs.2020.100225.
[23] O. Aydogdu, B. Burgu, P.U. Gocun, et al., Near infrared spectroscopy to diagnose experimental testicular torsion: comparison with doppler ultrasound and immunohistochemical correlation of tissue oxygenation and viability, J. Urol. 187 (2012) 744–750, https://doi.org/10.1016/j.juro.2011.09.145.
[24] F. Ufuk, D. Herek, Ö. Herek, et al., Diffusion-weighted imaging and color doppler ultrasound in evaluation of partial testicular torsion in rat model, Pol. J. Radiol. 82 (2017) 542–546, https://doi.org/10.12659/PJR.902613.

[25] A. Needles, A. Heinmiller, J. Sun, et al., Development and initial application of a fully integrated photoacoustic micro-ultrasound system, IEEE Trans. Ultrason. Ferroelectr. Freq. Control. 60 (2013) 888–897, https://doi.org/10.1109/TUFFC.2013.2646.
[26] A. Dolet, R. Ammanouil, V. Petrilli, et al., In vitro and in vivo multispectral photoacoustic imaging for the evaluation of chromophore concentration, Sensors 21 (2021) 3366, https://doi.org/10.3390/s21103366.
[27] M. Gerling, Y. Zhao, S. Nania, et al., Real-time assessment of tissue hypoxia in vivo with combined photoacoustics and high-frequency ultrasound, Theranostics 4 (2014) 604–613, https://doi.org/10.7150/thno.7996.
[28] L.B.E. Shields, M.W. Daniels, D.S. Peppas, et al., Testicular torsion in patients with intellectual and developmental disabilities, Glob. Pediatr. Health 8 (2021), 2333794X211059119, https://doi.org/10.1177/2333794X211059119.
[29] L.A. Baker, D. Sigman, R.I. Mathews, et al., An analysis of clinical outcomes using color doppler testicular ultrasound for testicular torsion, Pediatrics 105 (2000) 604–607, https://doi.org/10.1542/peds.105.3.604.
[30] L.B. Shields, M.W. Daniels, D.S. Peppas, et al., Sonography findings predict testicular viability in pediatric patients with testicular torsion, Cureus 14 (2022), e21790, https://doi.org/10.7759/cureus.21790.
[31] B. Zou, F. Zeng, Y. Yang, Using contrast-enhanced ultrasonography to assess the degree of acute testicular torsion: a case series, BMC Med. Imaging 22 (2022) 220, https://doi.org/10.1186/s12880-022-00953-9.
[32] P. Osemlak, G. Jędrzejewski, M. Woźniak, P, et al., Ultrasound evaluation of long-term outcome in boys operated on due to testicular torsion, Medicine 100 (2021), e26057, https://doi.org/10.1097/MD.0000000000026057.
[33] J. Chen, A.C. Sedgwick, S. Sen, et al., Expanded porphyrins: functional photoacoustic imaging agents that operate in the NIR-II region, Chem. Sci. 12 (2021) 9916–9921, https://doi.org/10.1039/d1sc01591e.
[34] C.A. DeMauro, M.M. Horrow, Diagnosis: incomplete testicular torsion progressing to complete torsion, Ultrasound Q. 24 (2008) 121–123, https://doi.org/10.1097/RUQ.0b013e31817b62b8.
[35] A. Laher, M. Swart, J. Honiball, et al., Near-infrared spectroscopy in the diagnosis of testicular torsion: valuable modality or waste of valuable time? A systematic review, Anz. J. Surg. 90 (2020) 708–714, https://doi.org/10.1111/ans.15402.
[36] B.J. Schlomer, M.A. Keays, G.M. Grimsby, et al., Transscrotal near infrared spectroscopy as a diagnostic test for testis torsion in pediatric acute scrotum: a prospective comparison to gold standard diagnostic test study, J. Urol. 198 (2017) 694–701, https://doi.org/10.1016/j.juro.2017.03.134.
[37] B. Burgu, O. Aydogdu, R. Huang, et al., Pilot feasibility study of transscrotal near infrared spectroscopy in the evaluation of adult acute scrotum, J. Urol. 190 (2013) 124–129, https://doi.org/10.1016/j.juro.2013.01.080.
[38] Z. Xie, Y. Yang, Y. He, et al., In vivo assessment of inflammation in carotid atherosclerosis by noninvasive photoacoustic imaging, Theranostics 10 (2020) 4694–4704, https://doi.org/10.7150/thno.41211.
[39] Y. Liu, H. Liu, H. Yan, et al., Aggregation-induced absorption enhancement for deep near-infrared II photoacoustic imaging of brain gliomas in vivo, Adv. Sci. 6 (2019), 1801615, https://doi.org/10.1002/advs.201801615.
[40] X. Liu, R. Gao, C. Chen, et al., Noninvasive photoacoustic computed tomography/ultrasound imaging to identify high-risk atherosclerotic plaques, Eur. J. Nucl. Med. Mol. Imaging 49 (2022) 4601–4615, https://doi.org/10.1007/s00259-022-05911-9.
[41] Y. Mantri, J.V. Jokerst, Impact of skin tone on photoacoustic oximetry and tools to minimize bias, Biomed. Opt. Express 13 (2022) 875–887, https://doi.org/10.1364/BOE.450224.
[42] W. Yim, J. Zhou, L. Sasi, et al., 3D-bioprinted phantom with human skin phototypes for biomedical optics, Adv. Mater. 35 (2023), e2206385, https://doi.org/10.1002/adma.202206385.

Mengyu Zhou received her B.S. in Biomedical mechanical engineering and automation from Shihezi University in 2020. Then she continued his studies at Guangzhou Medical University for a Master's degree in Biomedical Engineering. Her research interest is photoacoustic imaging.

Luting Zhang is in her third year of graduate studies in prenatal diagnosis and fetal medicine at The Third Affiliated Hospital of Guangzhou Medical University. Her main research interest is the application of photoacoustic imaging in diagnosis of diseases.

Jian-Wen Zeng is a professor at Guangzhou Medical University and director of urology at the Sixth Affiliated Hospital. His main research direction is the diagnosis and treatment of urinary system diseases.

Yintao Lan received his B.S. in Biomedical Engineering from Guangzhou Medical University in 2021. Then He continued his studies at Guangzhou Medical University for a Master's degree in Biomedical Engineering. His research interests are in optical imaging.

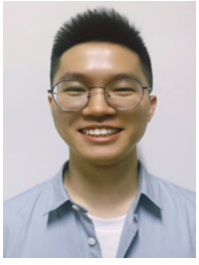

Fengbing He received his B.S. in Biomedical Engineering from Guangzhou Medical University in 2021. Then He continued his studies at Guangzhou Medical University for a Master's degree in Biomedical Engineering. His research interests are in biomedical photonics.

Weijian Gao is currently in his third year of graduate study in biomedical engineering at Guangzhou Medical University in Guangdong, China. The main research interest of Weijian Gao is now on biomedical photonics.

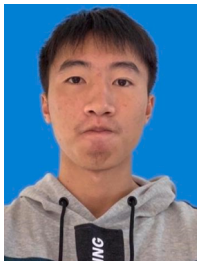

Jinghang Li is a third-year undergraduate in Biomedical Engineering School of Guangzhou Medical University, and his research field is medical optical imaging.

Qian Wang is currently a Lecturer at Guangzhou Medical University, China. She received the Ph.D. degree from Sun Yat-sen University, Guangzhou, China, in 2016. Her research interests include biomedical signal processing, body sensor networks, and pattern recognition.

Weisheng Guo is currently a professor in the School of Biomedical Engineering at Guangzhou Medical University. He received his Ph.D. from Tianjin University in 2015. His main research interests are construction of bionic intelligent nanomedicine and nanopharmacological evaluation.

Zhen Yuan is a professor in the Faculty of Health Sciences at University of Macau. His main research areas are as follows: Neuroscience and neuroimaging; Biomedical optics including functional near infrared spectroscopy, photoacoustic tomography/optoacoustic microscopy, optical coherence tomography.

Jian Zhang is a professor in the School of Biomedical Engineering at Guangzhou Medical University. He received his Ph. D. degree in optics from South China Normal University. He is a senior member of the Chinese Society of Biomedical Engineering. His main research field is developing optical imaging technology, and applying them in the clinical medicine.